AUTEX Research Journal, Vol. 20, No 1, March 2020 DOI: 10.1515/aut-2018-0058 © AUTEX

NUMERICAL SIMULATION OF THE CONDENSING EFFECT OF DIFFERENT SUCTION SLOTS ON FIBER STRANDS IN A COMPACT SIRO SPINNING MACHINE WITH LATTICE APRON

Chenchen Han[1], Weidong Gao[1,*], Lifen Chen[2]

[1]School of Textile and Clothing, Jiangnan University, Wuxi, Jiangsu 214122, People's Republic of China;
[2]Jiangsu Sunshine Group Co., Ltd., Jiangyin, Jiangsu 214426, People's Republic of China
*Corresponding author: Weidong Gao, e-mail: gaowd3@163.com

Abstract:

Compact-siro spun with lattice apron combines compact spinning and siro spinning, and is widely put into practice. In this paper, compact-siro spun models with the parallel shaped slots, oblique parallel shaped slots and V-shaped slots were simulated. Based on the airflow data in the condensing zone, the geometrical model of single fiber is built, and then the trajectory of single fiber can be got. The morphological changes and movement process of fiber strands in the flow field of condensing zone were verified by the comparison experiments of yarn morphology, hairiness, tensile and evenness properties. The results showed that the V-shaped slot achieved the optimal agglomeration effect and yarn performance. The theory analysis gives foundation and explanation for the experiment, and also provides a theoretical basis for optimizing the properties of compact-siro yarn in production practice.

Keywords:

compact-siro spun; flow field; numerical simulation

1. Introduction

Compact siro spun with lattice apron is a kind of new textile technology, which controls the two strands on the lattice apron by agglomeration and combines them into a more compact structure after gathering [1-3]. Compact siro spun with lattice apron, which is widely adopted in practice, attracts numerous career men's attention for its significantly enhanced yarn properties. Wang *et al.* [4] studied the causes of the increase in strength, the unevenness, and the decrease in hairiness for the compact siro yarn through a systematic theory analysis. They [5] further studied the factors that affect the yarn quality during the process of compact siro spinning. Lu *et al.* [6] evaluated the results of different suction slots by fuzzy mathematics and selected the suction installation by which yarns with the best comprehensive performances are spun. Current research on the spinning mechanism of compact siro spun technology, compact siro spun yarn structure, and the relationship between spinning process and yarn quality is not enough for optimizing the compact system and for improving compact technology. Liu *et al.* [7] studied the effects of lattice apron density on the yarn quality in a four-line compact spinning system by analyzing the numerical simulations of the airflow velocity; Akankwasa *et al*. [8] evaluated the dual-feed rotor spinning unit based on airflow dynamics and blended yarn properties; Jungbecker *et al*. [9] developed a kinematic model for yarn movement in turbulent airflows. These provide new research ideas and methods for the study of compact siro spun yarn. Therefore, several compact siro spun models with different arrangements of shaped slots are regarded as the subjects in this paper. Based on the results of simulation of airflow motion in the gathering area, the influences of airflow on fiber movement and the motion tracks of fiber strands were simulated by establishing an element model. Subsequently, the differences in the spun yarn performances were analyzed. The theoretical analysis gives the foundation and explanation for the experiment and also provides a theoretical basis for optimizing the properties of compact siro spun yarn in production practice.

2. Dynamic Model of the Single Fiber

2.1. Single-Fiber Model

Zou *et al*. [7] proposed a dynamic model of the infinitesimal element of the flexible fiber, which describes the flexible fiber trajectory in the condensing zone of compact spinning with a lattice apron. This paper mainly studies the compaction effect of fiber strands in the condensing zone. It needs to give more consideration to the lateral displacement of the fibers, and the bending properties of the fibers can be ignored. Accordingly, we choose the rigid infinitesimal segment as the single-fiber model. Assume that the fiber is composed of a series of rigid segments that have fixed length and quality [8]; then

$$\mathrm{d}m = \rho_f \frac{\pi}{4} d^2 \mathrm{d}l \tag{1}$$

where d*m* (cm) - the mass of the infinitesimal segment d*l*;

d*l* (cm) - the length of the infinitesimal segment;
r_f (g/cm^3) - the fiber's density;
d (cm) - the fiber's diameter.

2.2. Dynamic Analysis of the Single Fiber

Due to the complex state of fiber aggregation, the interaction of fibers will not be considered in the calculation process, and the heat exchange is also ignored. Considering that the output velocity of the fiber strands and the running velocity of the lattice apron are relatively static, the friction between the fiber strands and the lattice apron can be ignored during analysis.

Let us assume that the running time of the fiber's rigid infinitesimal segment *dl* in the condensing zone is *t* (s). In order to characterize the movement of *dl* at any time, the running time *t* can be averagely divided into *N* periods. The velocity of a rigid infinitesimal segment *dl* at any moment can be expressed as follows:

$$v_{it} = v_w \ (0 \le i \le N) \tag{2}$$

where v_w (cm/s) represents the running velocity of the lattice apron.

According to Newton's second law, the airflow force affecting the rigidity infinitesimal segment *dl* at time $i\Delta t$ in the *Z* direction can be expressed as follows:

$$\mathrm{d}m \cdot a_{zi} = \frac{1}{2} C_{Di} \rho_a v_{rzi}^2 \mathrm{d}A e_{rzi} \tag{3}$$

where a_{zi} (cm/s^2) - the acceleration of the infinitesimal segment d*l* at time $i\Delta t$ in the *Z* direction;

C_{Di} - the drag coefficient around flow at time $i\Delta t$;

r_a (g/cm^3) - the air density;

v_{rzi} (cm/s) - the relative velocity of the fibers and the flow in the *Z* direction;

dA (cm^2) - the area of facing flow;

e_{rzi} - the direction of the relative velocity v_{rzi}.

$$\mathrm{d}A = d \cdot \mathrm{d}l \tag{4}$$

where *d* (cm) - the fiber's diameter.

$$v_{rzi} = k \cdot V_{it} - v_{it} \tag{5}$$

where V_{zi} (cm/s) - the velocity of the flow in the *Z* direction at time $i\Delta t$;

v_{zi} (cm/s)- the velocity of the infinitesimal segment d*l* at time $i\Delta t$ in the *Z* direction;

k - the correction coefficient of the flow field, which depends on the permeability of the lattice apron [10].

The drag coefficient C_{Di} around the flow at time $i\Delta t$ is a function of the Reynolds number Re. It can be determined by C_D relative to the Reynolds number Re [9]. Re is defined as follows:

$$Re = \frac{v_{it} d}{\nu} \tag{6}$$

where v_{ri} (cm/s) - the relative velocity of the fibers and the flow at time $i\Delta t$;

v (cm/s) - the kinematic viscosity of air.

$$v_{it} = k \cdot V_i - v_i , \tag{7}$$

where V_i (cm/s) - the velocity of the flow at time $i\Delta t$;

v_i (cm/s) - the velocity of the infinitesimal segment d*l* at time $i\Delta t$.

The acceleration a_{zi} of the infinitesimal segment d*l* at time $i\Delta t$ in the *Z* direction can be defined as follows:

$$a_{zi} = \frac{2 C_{Di} \rho_a v_{rzi}^2}{\pi d \rho_f} e_{rzi} \tag{8}$$

The fibers in the compact direction are affected not only by the airflow force, but also by the friction force existing between the fibers and the lattice apron. According to Newton's second law, the force affecting the infinitesimal segment d*l* in the *Y* direction can be expressed as follows:

$$\mathrm{d}m \cdot a_{yi} = \frac{1}{2} C_{Di} \rho_a v_{ryi}^2 \mathrm{d}A e_{ryi} + f_i \tag{9}$$

where a_{yi} (cm/s^2) - the acceleration of the infinitesimal segment d*l* at time $i\Delta t$ in the *Y* direction;

v_{ryi} (cm/s) - the relative velocity of the fibers and the flow in the *Y* direction;

e_{ryi} - the direction of the relative velocity v_{ryi};

f_i - the friction force existing between the fibers and the lattice apron.

$$f_i = \mu \cdot N_{it} = \mu \cdot \mathrm{d}m \cdot a_{it} \tag{10}$$

where m - the friction coefficient between the fibers and the lattice apron;

$$v_{ryi} = k \cdot V_{it} - v_{it} \tag{11}$$

where V_{yi} (cm/s) - the velocity of the flow in the *Y* direction at time $i\Delta t$; and

v_{yi} (cm/s) - the velocity of the infinitesimal segment d*l* at time $i\Delta t$ in the *Y* direction.

The acceleration a_{yi} of the infinitesimal segment d*l* at time $i\Delta t$ in the *Y* direction can be defined as follows:

$$a_{it} = \frac{2 C_D \rho_a v_{ryi}^2}{\pi d \rho_f} e_{ryi} + \mu \cdot \frac{2 C_D \rho_a v_{rzi}^2}{\pi d \rho_f} e_{rzi} \tag{12}$$

According to the acceleration of the infinitesimal segment d*l,* which is obtained by calculations, the velocity at time $(i+1)\Delta t$ can be defined as follows:

$$v_{z(i+1)} = v_{\dot{z}} + \frac{\mathrm{d}v_{\dot{z}}}{\mathrm{d}t}\Delta t = v_{\dot{z}} + a_{\dot{z}}\Delta t \quad (13)$$

$$v_{y(i+1)} = v_{\dot{y}} + \frac{\mathrm{d}v_{\dot{y}}}{\mathrm{d}t}\Delta t = v_{\dot{y}} + a_{\dot{y}}\Delta t \quad (14)$$

The position coordinates of the infinitesimal segment d*l* in the flow field at time $(i+1)\Delta t$ can be expressed as follows:

$$Z_{i+1} = Z_i + \frac{\mathrm{d}Z_{i\to i+1}}{\mathrm{d}t}\Delta t = Z_i + v_{zi}\Delta t \quad (15)$$

$$Y_{i+1} = Y_i + \frac{\mathrm{d}Y_{i\to i+1}}{\mathrm{d}t}\Delta t = Y_i + v_{yi}\Delta t \quad (16)$$

$$X_{i+1} = X_i + v_{\dot{x}}\Delta t \quad (17)$$

On this basis, the trajectory of the infinitesimal segment d*l* in the flow field of condensing zone at time $i\Delta t$ can be expressed as follows:

$$\vec{S} = \vec{X}_i + \vec{Y}_i + \vec{Z}_i \quad (18)$$

3. Numerical Simulation

3.1. Three-Dimensional Geometric Model

The type of compact siro spun frame is Toyota RX240. In this paper, three different kinds of slots are mainly studied are reequipped based on it. Two strands get into the air gathering from the front roller nip zone parallelly at a constant pitch. There is a lattice apron on the outside surface of the shaped tube. The lattice apron drives by the friction of the output pressure top roller. It opens the suction slots on the spinning surface of the shaped tube. Inside the shaped tube, it is in negative pressure. The two strands output from the front roller are adsorbed on the lattice apron surface of suction slots. The two strands controlled by the agglomeration go forward on the lattice apron. They are output from the output pressure top roller. The two fiber strands obtain a more compact structure after gathering. After their respective initial twisting, the two fiber strands combine together, then are twisted strongly, and get a similar strand structure. An assembly drawing of every part in the condensing zone is shown in Figure 1.

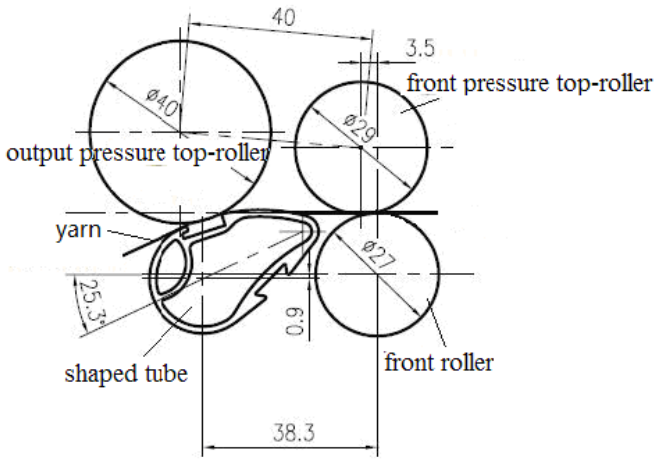

Figure 1. Machine drawing of compact siro equipment[7].

Xie *et al*. [1] developed 15 kinds of suction slots of different structures for compact siro spinning system installation. She evaluated the final result by fuzzy mathematics. The best suction pipe is that in which the suction notches have a symmetrical arrangement and are tilted at an angle of 6°; the yarn exportation spacing of the suction notches is 6 mm and the caliber size is small. This paper aims to compare the V-shaped slots, the parallel-shaped slots, and the oblique parallel-shaped slots shown in Figure 2. Based on the literature and existing models, we obtain the values as follows: *S*=1.40 mm; *L*=22.10 mm; *D*=4.00 mm; *a*=6°.

3.2. Solving Parameter Setting

Based on the previous results of gathering area airflow simulation [10], we set the solving parameters as follows. When calculating, we take the point O shown in Figure 3(a) as the origin of the coordinates, the opposite delivery direction of strand in the condensing zone is for the *X*-axis and the width direction of the slot is for the *Y*-axis. The *Z*-axis is perpendicular to the direction of strand movement. We have designed the three-dimensional geometric model using GAMBIT software, as shown in Figure 3(b). The spacing of the lattices is based on the interval size, and considering the time of simulation and the computer equipment, it chooses 0.35. The document is exported in the MESH format from GAMBIT, and the MESH document of GAMBIT is imported to FLUENT. Automatic control is used when refining by FLUENT. The ranges of the axes are set as follows: *X*-axis [0, 19]; *Y*-axis [–6, 12], and *Z*-axis [0, 3] in REGION [12]. As shown in Figure 3(b), the faces 1, 2, 3, 4, and 5 are specified as the pressure entrance faces, the face in the negative pressure area of the shaped tube is specified as the pressure exit face, and the others are specified as the wall [13]. The pressure entrance is at an atmosphere condition, and the exit is in a negative pressure (*P*=2.35 kPa). Because the negative values actually used are small, we suppose that the airflow in the condensing zone is sticky and incompressible. The heat exchange is ignored. The airflow is recognized to determine the enthalpy. So when calculating, the standard *k*-e turbulent model is applied [14]. When the convergence accuracy is 10^{-3}, the discrete scheme is changed from a first-order scheme to a second-order upwind scheme, and the convergence accuracy is set to be 10^{-4} [14]. The operation above is continued until it reaches the convergence accuracy needed.

3.3. Data Extraction

The distribution of velocity V_y in the *XY* plane in the condensing zones of the three different kinds of slots is shown in Figure 4. The data range is as follows: [–2.5, 18.5] in the *X* direction, and 33 points with 0.5 spacing are extracted; [–6, 12] in the *Y* direction, and 61 points with 0.3 spacing are extracted; [0, 1] in the *Z* direction, and 11 points with 0.1 spacing are extracted.

3.4. Parameter Setting

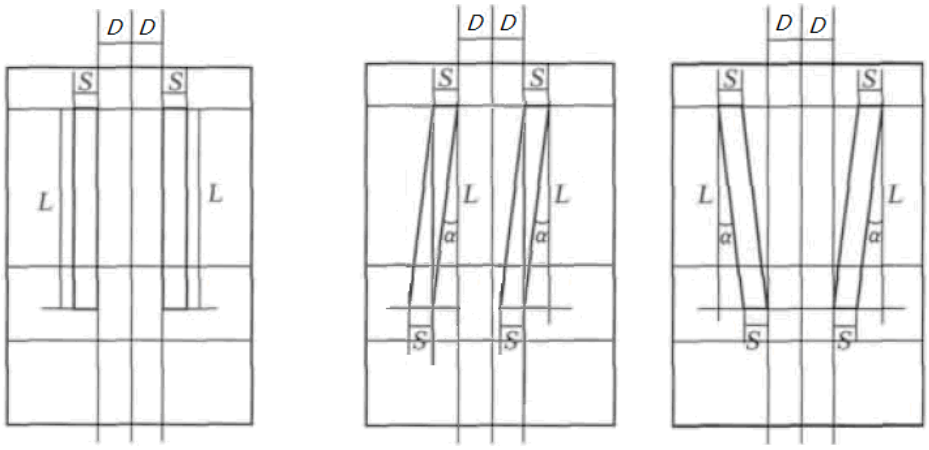

(a) parallel shaped slots (b) oblique parallel shaped slots (c) V-shaped slots

Figure 2. Shape and dimension of the suction slot [6].

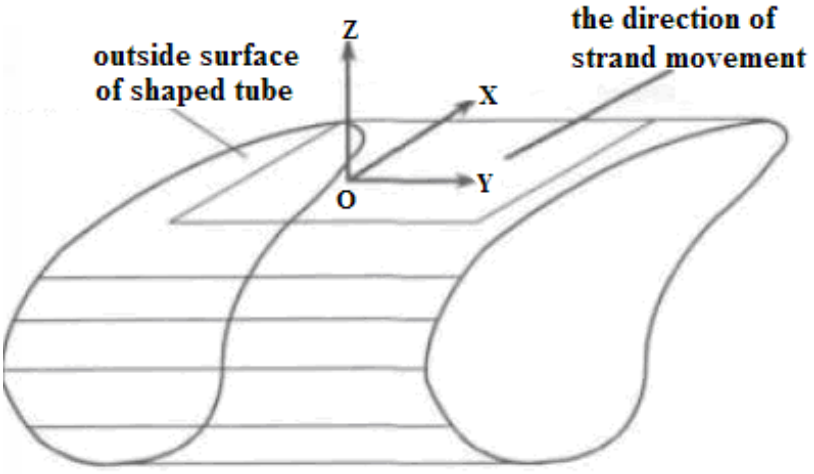

(a) Diagram of the velocity components direction.

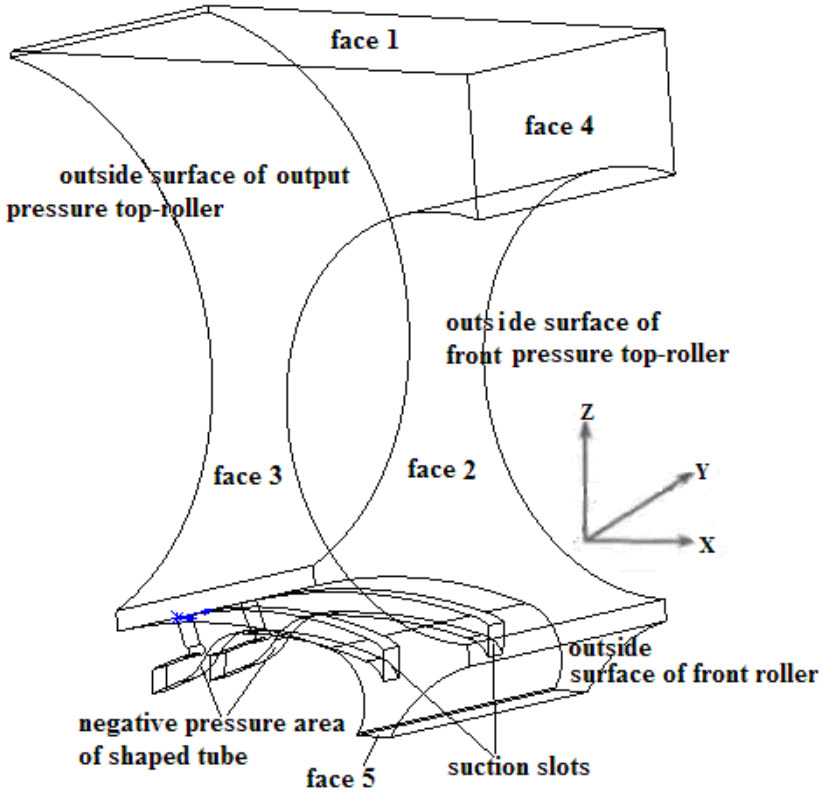

(b) Schematic diagram of flow field.

Figure 3. Schematic diagram of the structure of the compact siro zone.

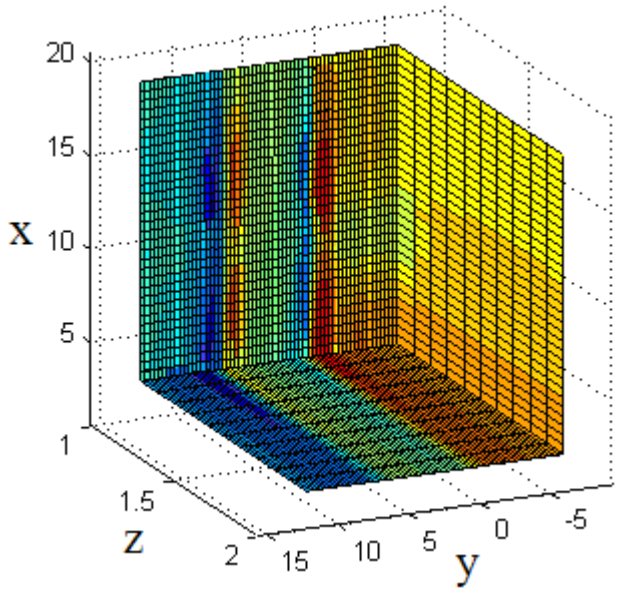

(a) Parallel shaped slots

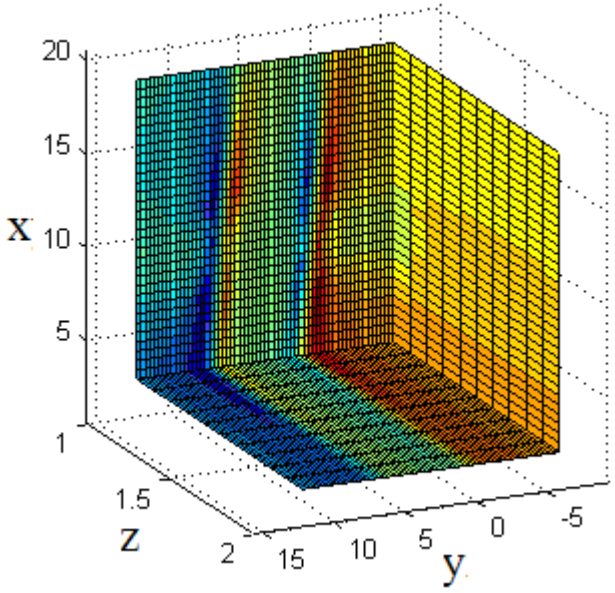

(b) Oblique parallel shaped slots

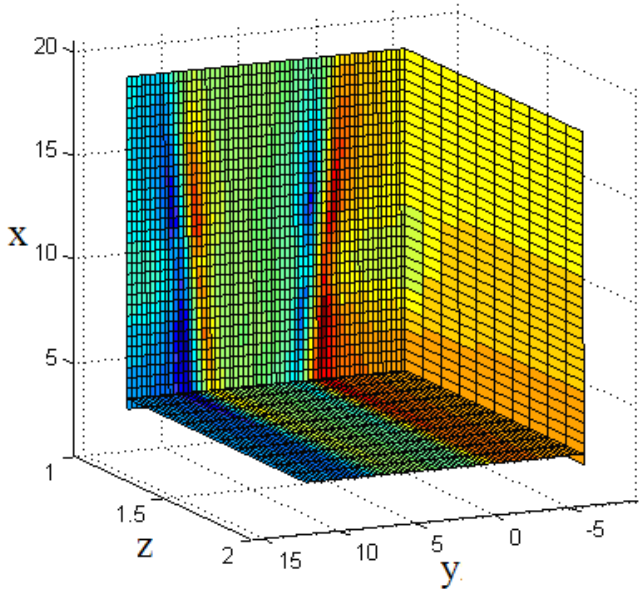

(c) V-shaped slots
Figure 4. Distribution of *Vy*.

The data of the flow field are input into MatLab, and the initial parameters of the fibers are designed. The trajectory of a single fiber in the condensing zone is calculated using the kinetic model, based on the data of airflow velocity in the condensing zone.

In order to combine the practical analysis, the model uses the trumpet, the spacing of which is 8 mm in this experiment. So, the spacing of the two strands when they enter the slot openings is 8 mm. The specific numbers of the motion parameters and the initial coordinates are as shown in Table 1 and Table 2: [6, 12] in the width direction *Y* of the fiber strands, and 10 initial positions y_0 with 0.6 mm spacing separation are extracted for each slot opening, which are symmetrical based on the middle of the two slot openings; [0, 1] in the height direction *Z* of the fiber strands, and four initial positions z_0 with 0.05 mm spacing separation are extracted; v_{x0}, v_{y0}, and v_{z0} are the initial velocities when the fibers get into the flow field of the condensing zone. Because V_x only affects the output speed of the fiber strands and does not affect the deflection, bending, and other movements of fibers in the condensing zone, to simplify the calculation, we need to ignore the force of V_x.

After the initial parameters are determined, according to the single-fiber model, first the velocity and the acceleration of the infinitesimal segment d*l* at any time is calculated, then the coordinates and the displacement, and finally the different initial positions of the single fiber's trajectory and the overall trajectory of the fiber strands in the condensing zone are obtained on the basis of these values.

3.5. Results and Analysis

As the airflow in the condensing zone facilitates the loose fiber strands to be compacted, the condensing effect of the airflow mainly occurred in the front area of the condensing zone, and in the latter area, we need to maintain the output status of the airflow. This paper mainly simulates the trajectory of the fiber in the condensing zone and compares the condensing effects.

Figure 5(a) shows the trajectory of the two fiber strands with spacing of 8 mm entering the condensing zone of the parallel-shaped slots from the two slot openings symmetrically. All the fibers get together at the point *X*=10 mm at roughly the same time. The fiber strands basically spread and are output from the center of the slot opening. The fibers exhibit torsion and tangled phenomena to a certain extent. The width of the fiber strand continues to decrease after gathering. The agglomeration effects on the S3 and S4 sides are much stronger than those on the S1 and S2 sides. Therefore, the total agglomeration effect on the yarn is ordinary.

Figure 5(b) shows the trajectory of the two fiber strands with spacing of 8 mm entering the condensing zone of the oblique parallel-shaped slots from the two slot openings symmetrically. As can be seen, the fibers close to the S1 and S2 sides get together at the point *X*=8 mm with other fibers. In addition, the remaining fibers gather at the point *X*=13 mm. The width of the fiber strand on the right slot continues to decrease after gathering. Because of the angle between the oblique parallel-shaped slots and the sliver conveying direction, the fiber strand

Table 1. Fibers' motion parameter setting

Direction (mm)	Positions
Parallel-shaped slots y_0	–4.04, –3.44, –2.84, –2.24, –1.64, –1.04, –0.44, 0.16, 0.76, 1.36; –1.36, –0.76, –0.16, 0.44, 1.04, 1.64, 2.24, 2.84, 3.44, 4.04
Oblique parallel-shaped slots y_0	–4.79, –4.19, –3.59, –2.99, –2.39, –1.79, –1.19, –0.59, 0.01, 0.61; –3.24, –2.64, –2.04, –1.44, –0.84, –0.24, 0.36, 0.96, 1.56, 2.16
V-shaped slots y_0	–4.04, –3.44, –2.84, –2.24, –1.64, –1.04, –0.44, 0.16, 0.76, 1.36; –0.64, –0.04, 0.56, 1.16, 1.76, 2.36, 2.96, 3.56, 4.16, 4.76
z_0	0.01, 0.06, 0.11, 0.16
x_0	0

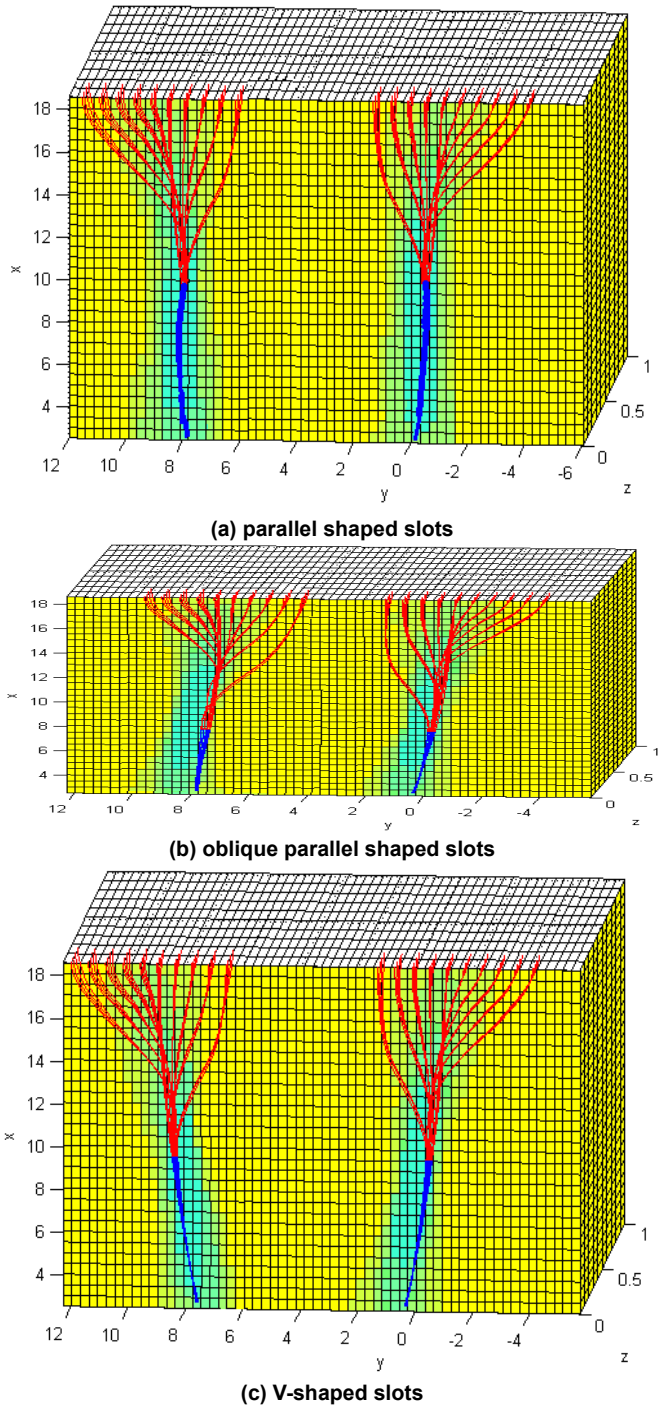

(a) parallel shaped slots

(b) oblique parallel shaped slots

(c) V-shaped slots

Figure 5. Trajectory of fibers.

Table 2. Fibers' initial parameter setting

Motion parameters	Value
Fiber diameter *d* (mm)	0.02
Fiber density r_f (g/cm^3)	1.54
Air density r_a (30°C) (kg/m^3)	1.165
Kinematic viscosity of air *n* (30°C) (m^2/s)	16.6×10^{-6}
Correction coefficient of the flow field, *k*	0.45
Number of time intervals, *n*	100
v_{x0} (m/s)	0
v_{y0} (m/s)	0
V_{z0} (m/s)	4

moves and outputs along the S2 side. The other fiber strand moves and outputs along the S3 side. The V_y on the sides of S1 and S2 are smaller than those on the sides of S3 and S4 though the data of the flow field show equal values; therefore, the agglomeration effect of the right slot is stronger than that of the left one. And the difference between the two fiber strands deteriorates the yarn quality.

Figure 5(c) shows the trajectory of the two fiber strands with spacing of 8 mm entering the condensing zone of the V-shaped slots from the two slot openings symmetrically. The two fiber strands gather at roughly the same time. The fibers close to the S1 and S2 sides get together at the point *X*=9 mm with other fibers. In addition, the remaining fibers gather at *X*=13 mm. The fiber strand basically moves along the center of the S4 side. The other fiber strand moves and outputs basically along the S3 side. The width of the fiber strand continues to decrease after gathering. The agglomeration effects of the V-shaped slots are basically the same and stronger. Therefore, the fibers in the yarn are close and flat, which greatly improves the yarn quality.

According to the simulation results and the analysis of the mechanism of fiber agglomeration, as the fibers enter the condensing zone, the strand is loose and its movement is unstable; the strands need larger *Vy* to be condensed and larger *Vz* to be adsorbed by a relatively stable negative pressure. It is revealed that the V-shaped slots are the best in terms of the agglomeration effect, and the oblique parallel-shaped slots are the worst.

4. Experiments

It is difficult to verify the agglomeration effect of the parallel-shaped slots, oblique parallel-shaped slots, and V-shaped slots directly, which are hence verified indirectly by the experiments on yarn structure and properties. To verify the simulation solution, the comparative experiments of yarn morphology, hairiness, tensile strength, and evenness properties were conducted at Ningbo Dechang Textile Machinery Limited Company. The experimental program according to the above theory is shown in Table 3. The raw material is cotton fiber, 38 mm × 1.33 dtex. The roving quantity is (0.42±0.02) g/m; the roving unevenness is £2%±0.1%; the roving moisture regain is 11.0%±0.5%. The environment of the workshop is under standard atmospheric conditions; the relative humidity is 65%±3%; the temperature is 20°C±2°C; the spindle speed is 14000 r/min; the total drafting ratio is 50; the drafting ratio at the back zone is 1.21; the roller diameters are 27 (mm) × 29 (mm) × 40 (mm); the wharve diameter is 22 mm; the ring diameter is 42 mm; the spacing between rovings before entering the front roller is 8.5 mm.

To evaluate the statistical significance of the difference between the slot structures, all data were analyzed using SPSS 16.0 statistical software (IBM Corporation, Somers, NY, USA). The results of breaking strength were analyzed using ANOVA. $P < 0.05$ was considered significant. As we can see from Table 4, the effects of the independent variables (such as yarn count and slot structure) on the dependent variable (such as breaking strength) are significant. According to the ANOVA test, the effects of independent variables such as yarn count and slot structure on the dependent variables such as tensile properties, hairiness properties, and evenness properties are also significant.

4.1. Yarn Morphology

The specimen was tested using a digital microscope KH-7700. Before testing, the specimen should be humidified for 48 hours at constant temperature and humidity in the laboratory: a temperature for (20±10) °C and a relative humidity for (65±15)% were used. The magnification was 250 times. The main observations included (a) not untwisted yarn; (b) partly untwisted yarn; and (c) untwisted yarn. The three morphological features are as shown below. It can be seen that the appearance of the yarn structure in V-shaped slots is the most compact, and that of yarn in the oblique parallel-shaped slots is the least.

Table 3. Spinning process parameters

Specimen	Spinning system	Yarn count, tex	Twist, T·m $^{-1}$	Negative pressure, Pa
1	Ring spinning	19.7	360	0
2	Compact siro spinning (parallel-shaped slots)	19.7	360	–1800
3	Compact siro spinning (oblique parallel-shaped slots)	19.7	360	–1800
4	Compact siro spinning (V-shaped slots)	19.7	360	–1800
5	Ring spinning	14.7	580	0
6	Compact siro spinning (parallel-shaped slots)	14.7	580	–2230
7	Compact siro spinning (oblique parallel-shaped slots)	14.7	580	–2230
8	Compact siro spinning (V-shaped slots)	14.7	580	–2230

Table 4. Result of analysis of variance (ANOVA) for breaking strength Dependent variable: breaking strength

Source	Type III sum of squares	df	Mean square	F	Significance
Corrected model	5489.157a	5	1097.831	28.787	0.001
Intercept	323851.735	1	323851.735	18682.032	0.000
Yarn count	4726.301	1	4726.301	90.882	0.000
Slot structure	644.000	2	322.000	18.575	0.002
Yarn count * slot structure	118.856	2	59.428	13.956	0.003
Error	624.085	15	41.606		
Total	330502.530	21			
Corrected total	6113.242	20			

Note: a. R-squared = 0.980 (adjusted R-squared = 0.957).

(a) Not untwisted yarn. (b) Partly untwisted yarn. (c) Untwisted yarn.

(1) parallel shaped slots

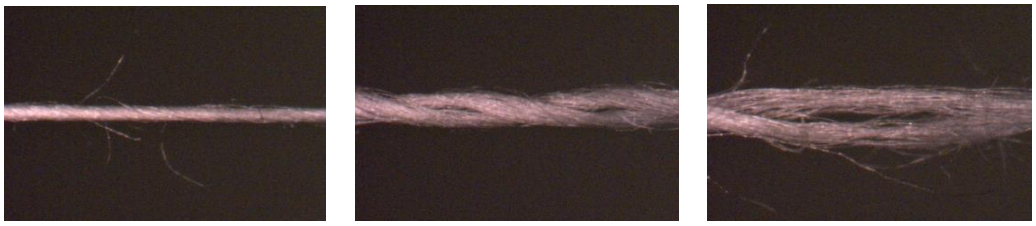

(a) Not untwisted yarn. (b) Partly untwisted yarn. (c) Untwisted yarn.

(2) oblique parallel shaped slots

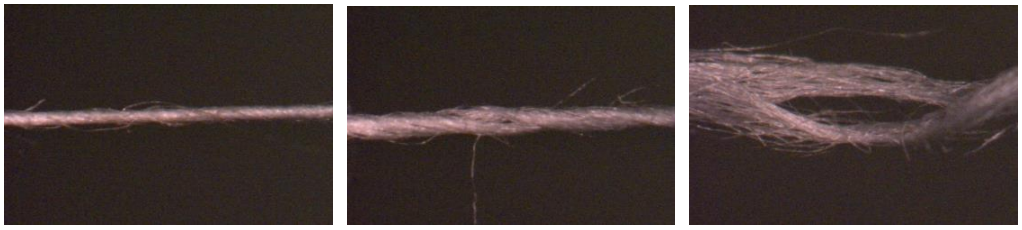

(a) Not untwisted yarn. (b) Partly untwisted yarn. (c) Untwisted yarn.

(3) V-shaped slots

Figure 6. The morphological features of yarn.

Table 5. Results of yarn hairiness properties

Specimen	1 mm	2 mm	3 mm	4 mm	5 mm	6 mm	7 mm	8 mm	9 mm
1	1382	234	101	53	22	11	8	1	1
2	839	121	38	7	1	1	1	1	1
3	932	157	58	18	6	2	2	1	1
4	724	136	37	4	1	1	1	1	1
5	509	118	45	13	5	2	1	1	1
6	448	87	16	5	1	1	1	1	1
7	496	93	19	5	2	1	1	1	1
8	338	55	12	2	1	1	1	1	1

4.2. Yarn Hairiness Properties

The specimen was tested using an YG172 yarn hairiness tester according to FZ/T1086-2000 standard. The pretension of yarn of different counts is adjusted by (0.5±0.1) cN/tex. The tested length is 10 m and the tested speed is 30 m/min. The tested specimens are six bobbins from different spindles, which have 10 replications per bobbin when tested.

In Table 5, on calculation, the harmful hairiness values (³3 mm) of specimen strands 2, 3, and 4 are 50, 88, and 46; the harmful hairiness values (³ 3mm) of 6, 7, and 8 are 26, 30, and 19. This is significant for the fabric appearance. For V-shaped slots, the harmful hairiness properties are the best among the three different kinds of slots, and those of the oblique parallel-shaped slots are the worst. The compact siro spinning can effectively control the hairiness induced by airflow and reduce the twist triangle. It can catch the harmful hairiness and wind it into the yarn. The V-shaped slots are more helpful for the hairiness to get compressed on the suction slots. The conclusion matches the results of numerical simulation well.

4.3. Tensile Properties of Yarn

Table 6. Results of yarn tensile properties

Specimen	Breaking strength, cN	Breaking tenacity, cN·tex^{-1}	Breaking elongation, %	Breaking work, cN·cm
1	428.6 (4.5)	21.7	6.7 (5.7)	79.8
2	541.8 (3.9)	28.9	7.3 (4.6)	123
3	483.3 (4.3)	25.5	7.2 (5.5)	99.8
4	589.1 (3.8)	33.3	7.5 (3.8)	131.7
5	255.9 (10.3)	11.5	5.7 (9.1)	29.5
6	340.1 (8.8)	19.2	6.2 (6.7)	58
7	290.8 (8.9)	16.7	5.8 (7.2)	43.8
8	388.9 (8.2)	24.7	6.3 (6..4)	61.2

Note: Data in parentheses are the coefficients of variation (CVs, %).

Table 7. Results of yarn evenness properties

Specimen	CVm, %	U, %	Thick places (+50%), km	Thin places (-50%), km	Neps (+200%), km
1	12.86	10.48	7	6	9
2	10.82	10.14	3	5	3
3	12.11	10.36	4	6	6
4	10.31	9.93	2	4	2
5	15.11	11.83	16	23	15
6	14.19	11.31	9	11	10
7	14.65	11.63	11	13	12
8	12.07	10.26	3	5	4

The specimen was tested using an YG068M automatic yarn tensor according to the standards GB/T398-2008, GB/T5324-2009, and so on. The pretension of yarn of different counts is adjusted by (0.5±0.1) cN/tex. The clamp distance is 0.5 m. The tested speed is 500 mm/min. The tested specimens are six bobbins from different spindles, which have 10 replications per bobbin when tested.

In Table 6, the breaking strength of Sample 3 reduces 10.8% compared with that of Sample 2 and reduces 17.9% compared with that of Sample 4. The breaking strength of Sample 8 increases 14.3% than that of Sample 6 and increases 33.7% relative to that of Sample 7. The breaking tenacity of Sample 3 reduces 11.7% compared to that of Sample 2 and reduces 23.4% compared to that of Sample 4#. The breaking tenacity of Sample 8 increases 28.6% compared to that of Sample 6 and increases 47.9% compared to that of Sample 7. The breaking elongation and breaking work basically have the same tendency. The compact siro spinning could reduce the spinning triangle caused by the airflow, so the fibers can be twisted almost at a horizontal position. It leads to a good fiber distribution in the yarn structure, which is approximately equal to the ideal model, and a highly effective utilization of single fiber. Meanwhile, the results of the tensile properties fit the results of numerical analysis: V-shaped slots are the best, parallel-shaped slots are better, and oblique parallel-shaped slots are the worst.

4.4. Evenness Properties of Yarn

The type of the yarn evenness test instrument is YG139D [15], and the test was conducted according to FZ/T1086-2000 standard. The pretension of yarn of different counts is adjusted by (0.5±0.1) cN/tex. During the yarn evenness test, the test speed is 400 m/min. The sampling time is 3 min. The tested specimens are six bobbins from different spindles, which have 10 replications per bobbin when tested.

In Table 7, on calculation, we find that the CVm of Sample 4 reduces 4.7% compared to that of Sample 2 and reduces14.9% compared to that of Sample 3. The CVm of Sample 8 reduces 14.9% compared to that of Sample 6 and reduces 17.6% compared to that of Sample 7. The U of Sample 4 reduces 2.1% compared to that of Sample 2 and reduces 4.2% compared to that of Sample 3. The U of Sample 8 reduces 9.3% compared to that of Sample 6 and reduces 11.8% compared to that of Sample 7. The thick places, thin places, and slubs basically have the same tendency. The compact siro spinning could reduce the spinning triangle by the twisting of the two fiber strands, which made the yarn have better evenness properties than the ring spun yarn. V-shaped slots could control the fiber ends more effectively and reduce the spinning triangle, so the fibers can be twisted almost at a horizontal position. The results of the evenness properties fit the tendency of numerical analysis.

5. Conclusions

In the context of the parallel-shaped slots, oblique parallel-shaped slots, and V-shaped slots, as the fibers enter the condensing zone, the strand is loose and its movement is unstable; they need a larger *Vy* to be condensed and a larger *Vz* – to be adsorbed by a relatively stable negative state – for the fibers of different initial positions, the deformed suction slot is better. The agglomeration effects of the V-shaped slots are basically the same and stronger. Therefore, the fibers in the yarn are close and flat, which greatly improves the yarn quality. By comparing yarn morphology, hairiness, tensile strength, and evenness properties of the different suction slots, it is found that the yarn of V-shaped slots has the best performance. So, a suction slot with symmetric configuration and smaller *D*, such as V-shaped slots, may have a better effect on the fiber strands.

Acknowledgments

This work was supported by the National Key R&D Program of China (2017YFB0309200); Natural Science Foundation of Jiangsu Province (BK20180582); Jiangsu Postdoctoral Research Funding Scheme (2018K019A); and Fundamental Research Funds for the Central Universities (JUSRP11801).

References

[1] *Xie C.P., Yang L.L., Su X.Z., Feng J. (2007). Analysis of compact effect and yarn structure of compact Siro spinning. Journal of Textile Research, 28(3), 9-12.*

[2] *Cheng K.P.S, Yu C. (2003). A study of compact spun yarns. Textile Research Journal, 73(4), 345-349.*

[3] *Qin Z.J., (2006). The technology of spinning elitist ply yarn. Shandong Textile Science & Technology, (1), 7-10.*

[4] *Wang W.Y., Zou Z.Y., Hua Z.H., Zhu Y.D., Cheng L.D. (2009). Simulation and analysis of trajectory of fiber in condensing zone of compact spinning with lattice apron. Journal of Textile Research, 30(10), 48-52.*

[5] *Wang Y.F., Gu P., Gu B.P. (2010). Comparison of properties of yarns spun by compact-siro, siro and compact spinning. Advanced Textile Technology, (6), 1-3.*

[6] *Lu L.F., (2013). Study on the condensing mechanism and key components of compact-siro spun with lattice apron. MD Thesis, Donghua University, China.*

[7] *Liu X.J., Su X.Z., Zhang H. (2016). Effects of lattice apron density on yarn qualities in Four-line compact spinning system. The Journal of The Textile Institute, 108(4), 511-521.*

[8] *N.T. Akankwasa, Lin H., Wang J. (2017). Evaluation of the dual-feed rotor spinning unit based on airflow dynamics and blended yarn properties. The Journal of The Textile Institute, 108(11), 1985-1996.*

[9] *P. Jungbecker, G. Seide, T. Gries. (2008). Kinematic model for yarn movement in turbulent air flows. Autex Research Journal, 8(4), 94-99.*

[10] *Zou Z.Y., Zhu Y.D., Hua Z.H., Wang Y., Cheng L.D., (2010). Studies of flexible fiber trajectory and its pneumatic condensing mechanism in compact spinning with lattice apron. Textile Research Journal, 80(8), 712-719.*

[11] *Chiba K., Komatsu T. (2007). Numerical simulation for orientation of thin disk particles in a newtonian flow through a l-shape channel. Journal of Textile Engineer, 50(1), 31-35.*

[12] *Wang Y., Hua Z.H., Cheng L.D., Xue W.L. (2009). Influence of processing parameters on quality of fiber compact in condensing zone of compact spinning with lattice apron. Journal of Textile Research, 31(2), 27-32.*

[13] *Han C.C., Wei M.Y., Xue W.L., Cheng L.D. (2015). Numerical simulation and analysis of airflow in the condensing zone of compact-siro spinning. Textile Research Journal, 85(14), 1506-1519.*

[14] *Xue W.L., Wei M.Y., Wang Y., Cheng L.D., Zhang R.Y. (2011). Comparison of flow field distribution and characteristic on different compact spinning systems. Journal of Donghua University (English Edition), 85(14), 326-330.*

[15] *Zou Z.Y., Wang Y., Yu J.Y., Zhu Y.D., Wu J.N., Cheng L.D. (2009). Characterization and analysis of three-dimensional flow field in compact spinning with lattice apron. Journal of Textile Research, 31(6), 24-28.*

[16] *Zhang N., Xue W.L., Cheng L.D. (2012). Simulation and analysis on condensing effect of the different air suction slots of compact spinning with lattice apron. Journal of Donghua University (English Edition), 85(2), 160-163.*

[17] *Zhang N. (2012). Study on the Simulation about Condensing Process and Addition Twist of Compact Spinning with Lattice Apron. MD Thesis, Donghua University, China.*

[18] *Xu S.D., Wang X. (2012). Discussion on two methods evaluation yarn evenness. Cotton Textile Technology, 12, 29-31.*